General Disclaimer

One or more of the Following Statements may affect this Document

- This document has been reproduced from the best copy furnished by the organizational source. It is being released in the interest of making available as much information as possible.

- This document may contain data, which exceeds the sheet parameters. It was furnished in this condition by the organizational source and is the best copy available.

- This document may contain tone-on-tone or color graphs, charts and/or pictures, which have been reproduced in black and white.

- This document is paginated as submitted by the original source.

- Portions of this document are not fully legible due to the historical nature of some of the material. However, it is the best reproduction available from the original submission.

NASA Technical Memorandum 83351
E-A-83-0762

Cross Spectra Between Temperature and Pressure in a Constant Area Duct Downstream of a Combustor

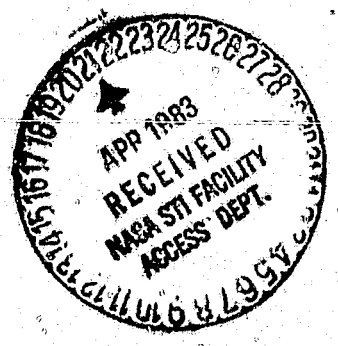

J. H. Miles, C. A. Wasserbauer, and E. A. Krejsa
Lewis Research Center
Cleveland, Ohio

Prepared for the
Eighth Aeroacoustics Conference
sponsored by the American Institute of Aeronautics and Astronautics
Atlanta, Georgia, April 11–13, 1983

NASA

CROSS SPECTRA BETWEEN TEMPERATURE AND PRESSURE IN A CONSTANT AREA DUCT DOWNSTREAM OF A COMBUSTOR

J. H. Miles, C. A. Wasserbauer and E. A. Krejsa

National Aeronautics and Space Administration
Lewis Research Center
Cleveland, Ohio 44135

Abstract

Theory indicates that pressure-temperature cross-spectra are necessary in predicting noise in regions of velocity gradients. In the present study, the feasibility of measuring pressure-temperature cross-spectra and coherence and temperature-temperature cross-spectra and coherence at spatially separated points along with pressure and temperature auto-spectra in a combustion rig was investigated. The measurements were made near the inlet and exit of a 6.44 m long duct attached to a J-47 combustor. For this study the fuel used was Jet A. The cross-spectra and coherence measurements show the pressure and temperature fluctuations correlate best at low frequencies. At the inlet the phenomena controlling the phase relationship between pressure and temperature could not be identified. However, at the duct exit the phase angle of the pressure is related to the phase angle of the temperature by the convected flow time delay.

Nomenclature

c_o	speed of sound
c_p	specific heat at constant pressure
f	frequency
G_{ii}	thermocouple auto-spectrum
G_{ij}	thermocouple cross-spectrum
H_{ii}	ratio of thermocouple auto-spectrum to cross-spectrum, G_{ii}/G_{ij}
i	$\sqrt{-1}$
k	wavenumber, ω/c_o
n	integer
p	acoustic pressure
R	duct exit reflection factor
S	entropy perturbation
T	temperature perturbation
W	mass flow rate
x	displacement of point from combustor entrance
γ	ratio of specific heats
σ	square root of the variance of a distribution
τ	thermocouple time constant
ω	angular frequency, $2\pi f$

Superscripts:

*	complex conjugate
'	perturbation

Subscripts:

g	gas
m	measured
1,2	thermocouple number
3,4	duct locations

Introduction

A program to study turbofan engine core noise has been conducted at the NASA Lewis Research Center. In the study of core noise, the influence of combustion must be considered because the combustion process is a major source of noise from a turbofan engine core. In a combustor, fluctuations in the heat release rate can cause both entropy and pressure perturbations. The pressure waves propagate through the engine and are radiated to the far field. The entropy variations are not direct noise sources because they have no associated pressure disturbance. However, as the entropy convects through regions of velocity gradients they, too, generate acoustic waves. The resulting combustion noise represents a combination of waves due to both sources.

A model for predicting noise propagation in a variable area core nozzle which included convected entropy is discussed in Ref. 1. Using this model, calculations show that the noise level at a given frequency can be related to the entropy auto-spectrum. Furthermore, the core nozzle transfer function is affected by the entropy-pressure cross spectrum. The calculations show that if the entropy and pressure are in phase at the inlet, the magnitude and phase of the transfer function can have a rippled appearance. Consquently, in order to describe certain characteristics of combustion noise propagation, information about the cross-spectrum between the convected entropy and pressure and the entropy auto-spectrum are required. However, no experimental entropy auto-spectra or entropy-pressure cross-spectra were available to use in the model.

An entropy perturbation, S', is related to a perturbation in gas pressure, p', and temperature, T' by

$$\frac{S'}{c_p} = \frac{T'}{T_o} + \frac{(1-\gamma)}{\gamma}\frac{p'}{p_o} \qquad (1)$$

Thus in order to obtain the entropy auto-spectrum and the entropy-pressure cross spectrum the temperature and pressure auto-spectra as well as the temperature-pressure cross-spectrum must be measured. The purpose of this paper is show that it is feasible to measure temperature-pressure cross-spectra in a combustion rig over a range of frequencies of interest in combustion noise studies, to obtain some baseline data, and to determine if some non-random phase relationship, as hypothesized in Ref. 1, between pressure and temperature can exist.

Dynamic temperature and pressure measurements have been made in combustors[2-5] in order to obtain auto-spectra. In this paper an exploratory study investigating the measurement inside a combustion rig of pressure-temperature cross-spectra and coherence at a single point as well as temperature cross-spectra and coherence at spatially separated points is presented. Pressure and temperature auto-spectra inside the combustion rig are also obtained. The engineering data acquired

can be used in models, such as that discussed in Ref. 1, and compared with other published results.

The measurements to be described were made in a long (6.44 m) constant area duct attached to a J-47 combustor. The rig was designed to operate with no combustion in the long duct. However, for all the test conditions some combustion did occur at the duct inlet station where one set of pressure and temperature measurements were made.

Experimental Apparatus

The temperature and pressure measurements were made in the combustion rig shown in Fig. 1 which consisted of a J-47 can combustor (see Fig. 1(b)) mounted in a 0.3 m diameter by 0.77 m long test section and an attached 6.44 m long 0.3 m diameter stainless steel duct. The fuel used was Jet A. This paper discusses pressure and temperature measurments at stations 3 and 4. The test conditions are shown in Table I.

All tests were conducted in an outdoor acoustic arena. The facility is shown in Fig. 2.

Note that in all cases the duct exit temperature was greater than the duct inlet temperature indicating some combustion was occuring in the duct. This was due to mechanical problems which developed in the combustor during the test program. These problems make the test conditions difficult to duplicate and hinder the interpretation of the measurements. However, the combustor mechanical problems have no bearing on the examination of the feasibility of measuring temperature-pressure cross spectra.

Pressure Measurements

The internal pressure transducers used were conventional 0.635 cm microphones with pressure response cartridges. In order to avoid direct exposure of the microphone to the combustion gases, they were mounted outside the ducted combustion rig and the fluctuating pressure in the rig was transmitted to the transducers by means of a "semi-infinite" acoustic wave guide. Details on these probes are given in Ref. 6.

Temperature Measurements

The temperature fluctuations were measured using chromel-alumel thermocouples. The two wire thermocouple probe design shown in Fig. 3 was selected so that the response time of the thermocouple could be determined based on the actual test data, as opposed to a separate precalibration. The procedure discussed in Ref. 7 was used. The thermocouple chromel-alumel wire diameters were 76.2 and 25.4 μm. The thermocouples were inserted into the duct by actuators after combustion started in order to prevent their destruction by the combustion start up transient. While the thermocouples were quite durable, their lifetime was drastically reduced by operation at elevated temperatures (1115 K).

The approach used to determine the themocouple time constants is based on the two thermocouple method described in Ref. 7 However, the actual time constants were not found by examination of the plots as suggested in Ref. 7. Instead, a nonlinear minimization technique was used to find the time constants to minimize the least square error between the measured and theoretical values of H_{11} and H_{22} where

$$H_{11} = \frac{G_{11}}{G_{12}} = \frac{1 + \omega^2\tau_1\tau_2 + i\omega(\tau_1 - \tau_2)}{1 + \omega^2\tau_1^2} \qquad (2)$$

and

$$H_{22} = \frac{G_{22}}{G_{11}} = \frac{1 + \omega^2\tau_1\tau_2 + i\omega(\tau_1 - \tau_2)}{1 + \omega^2\tau_2^2} \qquad (3)$$

where

$$i = \sqrt{-1}$$

The temperature auto-spectra are G_{11}, and G_{22} and the temperature-temperature cross spectrum is G_{12}. The model used assumes that the measured temperature, T_m, is related to the gas temperature, T_g by

$$T_m = \frac{T_g}{1 + i\omega\tau} \qquad (4)$$

in the frequency domain. Futhermore, it is assumed that the coherence between the two thermocouples is high so that extraneous noise can be neglected.

Examination of the plots of the real and imaginary values of H_{ij} can yield information on the time constants since the imaginary value of H_{ij} has a maximum at $\omega = 1/\tau_j$. Furthermore

$$\lim_{\omega\to\infty} H_{11} = \tau_2/\tau_1 \qquad (5)$$

and

$$\lim_{\omega\to\infty} H_{22} = \tau_1/\tau_2 \qquad (6)$$

The time constant in all cases was determined using the spectrum between 0 and 40 Hz.

In order to demonstrate the procedure, typical constant bandwidth (0.08 Hz) two wire thermocouple auto-spectra, cross-spectra and coherence function measurements are shown in Figs. 4 to 8. Note that the thermocouple coherence is high (Fig. 6). This is a necessary condition for application of the calibration procedure since it means that extraneous noise is low. In addition, the measured values of H_{11} and H_{22} are shown in terms of their real and imaginary components along with the least square curve fits used to find the time contants (Figs. 7 and 8). The $\omega = 1/\tau_j$ points and the high frequency asymptotic value of H_{ij} are also identified. Also, in Fig. 4 the gas temperature, T_g, auto-spectrum and cross-spectrum after correction are shown. Table I gives the time constants used to correct the cases used herein.

Results and Discussion

This section discusses measurements of pressure-pressure and temperature-temperature cross-spectra between the inlet and the exit of

the long duct. Also, pressure-temperature cross-spectra at the inlet and the exit of the duct are discussed. Only, a few typical results sufficient to establish definite trends are included here.

With each cross-spectrum, the corresponding coherence function is presented. Note that a coherence smaller than unity implies one or more of the following conditions exists:

1. Extraneous noise is present in the measurements.
2. The system relating the output to the input is non-linear.
3. The output is due to more than one input.

Pressure Cross-Spectra and Auto-Spectra

Typical constant bandwidth (2 Hz) pressure to pressure cross-spectra and pressure auto-spectra are shown in Figs. 9 to 11. The cross-spectra magnitude plots and auto-spectra magnitude plots have certain similarites since as the temperature increases, the frequency at which a particular spectral feature occurs increases in a proportion that keeps the wave number constant. However, the variation in temperature along the duct produces distortions in the shape of the magnitude plot that would not appear in a constant temperature duct. The pressure auto-spectra are shown so that they can be compared with the corresponding temperature-pressure cross-spectra.

The cross-spectra phase relationships are due to a longitudinal standing wave in the duct. The cross-spectra phase angle is intially zero corresponding to a positive value of $p_3p_4^*$. The phase angle switches by 180 degrees at approximately 50 Hz intervals. The phase angle variaton with frequency of the pressure cross spectra in the duct is understandable in terms of a simple no flow model for the acoustic pressure distribtion in the duct. Without flow the pressure in the duct is proportional to

$$p = e^{ikx} + R\, e^{-ikx} \qquad (7)$$

Furthermore, at low frequencies the reflection factor is nearly - 1. Consequently, the pressure is approximately proportional to $\sin(kx)$. Thus the pressure cross-spectrum between station 3 and 4, $p_3p_4^*$, in a duct without flow is then proportional to

$$p_3p_4^* = \sin(kx_3)\sin(kx_4) \qquad (8)$$

where $x_3 = 1.47$ m and $x_4 = 6.91$ m. This function is either positive or negative and it changes sign at frequencies n_f which are multiples of the first zero of $p_3p_4^*$. The phase angle deviations from this simple model are due to the presence of flow and the duct reflection and the duct reflection factor not being -1.

The corresponding coherence functions are shown in Fig. 12. The coherences are quite large above 20 Hz. However, at multiples of the first zero of $p_3p_4^*$ the coherence is zero.

Temperature-Temperature Cross-Spectra

Temperature-temperature constant bandwidth (0.4 Hz) cross-spectra between the entrance and the exit of the duct are shown for three cases in Fig. 13. All temperature measurements are shown after correction The cross-spectrum magnitude is largest at low frequencies.

At low frequencies (up to 50 Hz) the phase of the cross spectra changes linearly with frequency with slopes proportional to the time delay due to convection of temperature in the duct. The time delay is about 125 ms for the data shown in Figs. 13(a) and (b) where the mass flow rate, W, is 0.5 kg/s and 62.5 ms for the data shown in Fig. 13(c) where the mass flow rate is 1.13 kg/s.

The corresponding coherence data are shown in Fig. 14. At the higher frequencies the coherence is very low (Fig. 14) and no orderly relationship between the temperatures is observed. Note also, from Fig. 14, that as the amount of burning in the duct increases the coherence is greatly reduced.

The thermocouple signals show the presence of 60 Hz and 110 Hz noise. The signal at station 4 at the duct exit was more contaminated than the signal at station 3 at the duct inlet.

Pressure-Temperature Cross-Spectra

Duct inlet: Pressure-temperature constant bandwidth (0.40 Hz) cross-spectra at the duct inlet (station 3) for three cases are shown in Fig. 15. The corresponding coherence fuctions are shown in Fig. 16. The mechanical cut-off frequency of the microphone due to pressure equalization is abcut 5 Hz. Consequently, below this frequency the data are unreliable.

Above 50 Hz the shapes of the pressure-temperature cross-spectra magnitude plots (Fig. 15) resembles the shapes of the corresponding pressure auto-spectra magnitude plots shown in Fig. 10. This indicates that the part of the temperature perturbation coherent with the pressure perturbation has no strong spectral characteristics above 50 Hz.

The phase angle variation shows distinct patterns, indicating a systematic relationship between pressure and temperature near the source region. However, the physical phenomena producing this pattern have not been identified.

Comparing, the pressure-temperature cross-spectrum magnitude plots (Fig. 15) and coherence plots (Fig. 16) with the pressure auto-spectra plots (Fig. 10) shows that the temperature perturbation is weakly excited in certain frequency bands near particular duct resonant frequencies. For inlet temperatures of 1115, 875 and 920 K note the 110 Hz, 98 and 70 Hz regions respectively.

The systematic relationship between the pressure and the temperature at the inlet is not a strong one. Consequently, it is more visible in the phase plots than the coherence plots.

Duct exit: Pressure-temperature constant bandwidth (0.40 Hz) cross-spectra at the duct exit (station 4) for three cases are shown in Fig. 17. The corresponding coherence fuctions are shown in Fig. 18. Again the magnitude plots of the pressure-temperature cross spectra resemble the magnitude plots of the corresponding pressure auto-spectra shown in Fig. 11.

The phase of the cross spectra again show linear dependence with slopes that are proportional to the time delay due to convection of temperature in the long duct. Note, that since this is a phase measurement between two different variables, that is pressure and temperature, at the same point, the time delay must be due to the difference in travel times between a pressure and temperature disturbance as they travel from the same upstream source region. This shows that temperature and pressure fluctuations are related at the combustion source point. Furthermore, an extrapolation of the cross-spectrum suggests that the two are in phase at low frequencies.

In view of these findings that pressure and temperature are in in phase at the source in this combustion rig, it is possible that the entropy and pressure in the JT15D nozzle might also be in phase at the nozzle inlet. Thus, some of the ripple in the measured JT15D transfer function presented in Ref. 1 might be due to convected entropy. This suggests that it might be of interest to obtain dynamic temperature measurements along with acoustic pressure measurements in turbofan engine tests.

Temperature Auto-Spectra

Because plots of the gas temperature auto-spectra resemble those presented in Fig. 5, additional ones are not included. It can be seen that most of the fluctuations are at low frequencies. The temperature standard deviations calculated by integrating the temperature auto-spectra for a frequency range from 0 to 200 Hz are shown in Table I. The percent r.m.s. temperature fluctuations are also shown in Table I. At the inlet where combustion is occuring they vary in a range from 15 to 20 percent. At the duct exit the range is 2 to 4 percent. These results are similar to those found at the exit of the gas turbine combustor by Dils[2] where the per cent r.m.s. temperature fluctuations were 7 and 10 percent at a takeoff operating condition where the average temperatures were 1430 and 1438 K. The burner exit r.m.s. temperature fluctuations reported in Ref. 5 are generally lower than those observed by Dils.

Conclusions

From the results of this exploratory study, the following conclusions were reached:

1. Pressure and temperature cross-spectra and coherence functions can be measured in a combustion rig using a two-wire thermocouple probe and an infinite tube microphone over a range of frequencies of interest in combustion noise studies.

2. The temperature and pressure fluctuations are related at the combustion source point and an extrapolation of the cross-spectrum phase suggests that the two are in phase at low frequencies.

3. At the duct exit the phase angle of the pressure is related to the phase angle of the temperature by the convected flow time delay.

These three conclusions, taken together, provide confidence that identifiable physical relationships between temperature and pressure in a combustion system can be measured using sophisticated data analysis techniques. These relationships are valuable either as inputs or as verification of outputs of theoretical models describing combustion noise generation or propagation.

References

1. Miles, J. H., and Krejsa, E. A., "Pressure Transfer Function of a JT15D Nozzle Due to Acoustic and Convected Entropy Fluctuations," Journal of the Acoustical Society of America, Vol. 72, Dec. 1982, pp. 2008-2019.

2. Dils, R. R., "Dynamics Gas Temperature Measurements in a Gas Turbine Transtion Duct Exit," Journal of Engineering for Power, Vol. 95, No. 3, July 1973, pp. 265-277.

3. Muthukrishnan, M., Strahle, W. C., and Neale, D. H., "Separation of Hydrodynamic, Entropy, and Combustion Noise in a Gas Turbine Combustor," AIAA Journal, Vol. 16, No. 4, Apr. 1978, pp. 320-327.

4. Sofrin, T. G., and Riloff, Jr., N., "Experimental Clean Combustor Program-Noise Study," Pratt and Whitney Aircraft, East Hartford, Conn., PWA-5458, Sept. 1976. (NASA CR-135106.)

5. Mathews, D. C., Rekos, Jr., N. F., and Nagel, R. I., "Combustion Noise Investigation-Predicting Direct and Indirect Noise from Aircraft Engines," Pratt and Whitney Aircraft Group, PWA-5478, FAA-RD-77-3, Feb. 1977.

6. Karchmer, A. M., and Reshotko, M., "Core Noise Source Diagnostics on a Turbofan Engine Using Correlation and Coherence Techniques," NASA TM X-73535, 1976.

7. Strahle, W. C., and Muthukrishnan, M., "Thermocouple Time Constant Measurement by Cross Power Spectra," AIAA Journal, Vol. 14, No. 11, Nov. 1976, pp. 1642-1644.

TABLE I. - THERMOCOUPLE TIME CONSTANTS, TEMPERATURE STANDARD DEVIATION, AND RMS TEMPERATURE FLUCTUATION

Test Point	87	86	88
T_{exit}, K	1135	990	1120
T_{inlet}, K	1115	875	920
W, kg/s	0.5	0.5	1.13
Time constant			
Station 4 (exit)			
τ_1 (76.2 μm diam), ms	41	79	49
τ_2 (25.4 μm diam), ms	20	34	22
Station 3 (inlet)			
τ_1 (76.2 μm diam), ms	61	67	42
τ_2 (25.4 μm diam), ms	36	40	25
Standard temperature deviation, σ			
Station 4 (exit), K	35	40	25
Station 3 (inlet), K	170	150	170
Percent rms temperature fluctuation			
Station 4 (exit)	3	4	2
Station 3 (inlet)	15	17	19

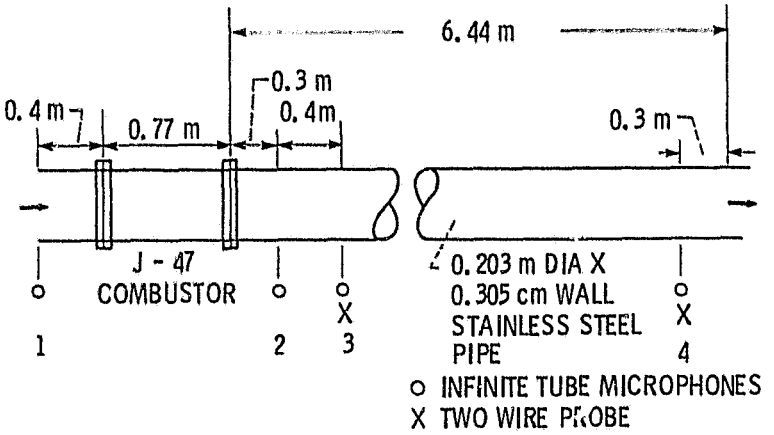

(a) Rig schematic.

Figure 1. - Schematic of ducted combustion system rig.

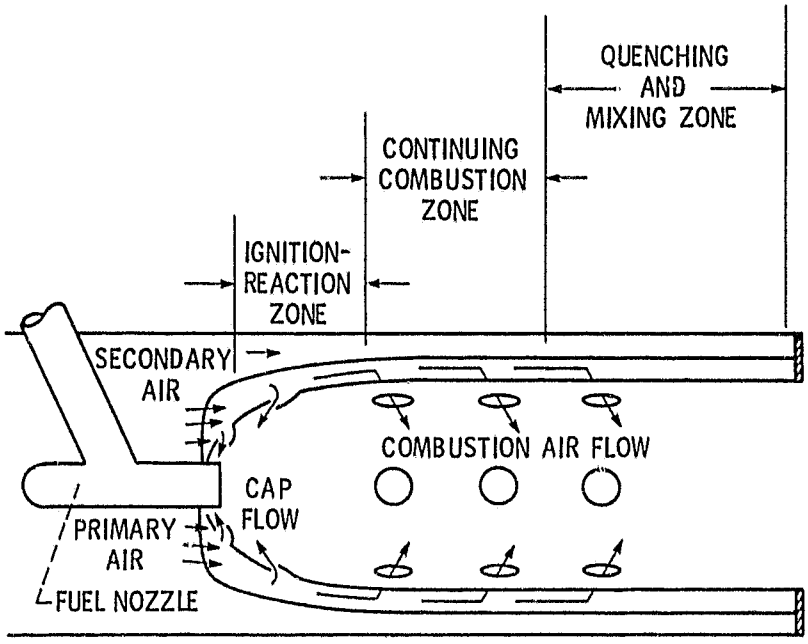

(b) Injection scheme.

Figure 1. - Concluded.

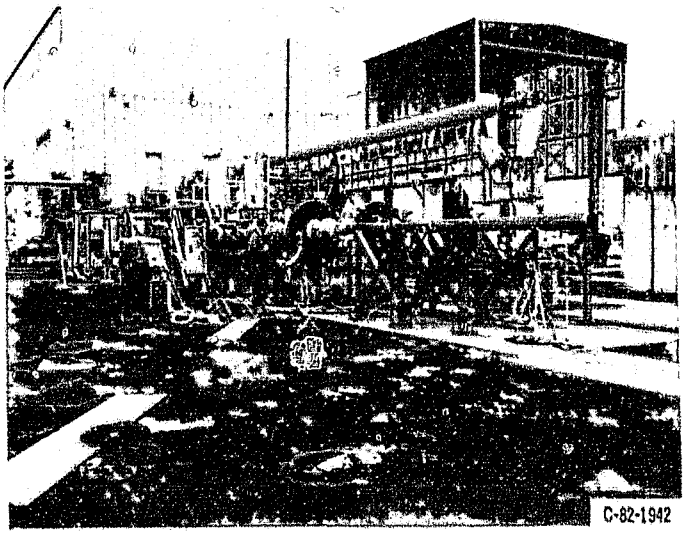

Figure 2. - NASA Lewis combustion acoustics facility.

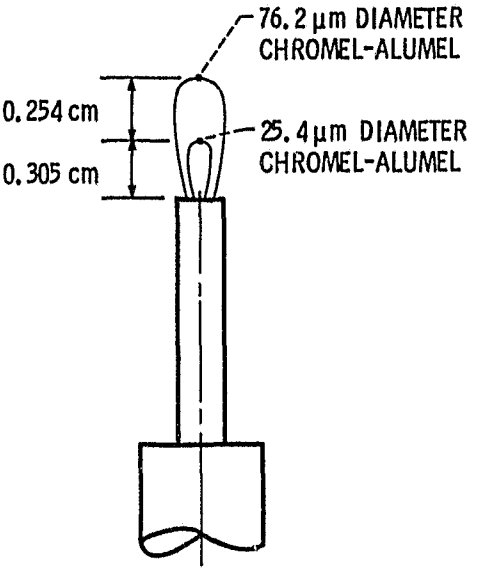

Figure 3. - Two wire thermocouple probe design.

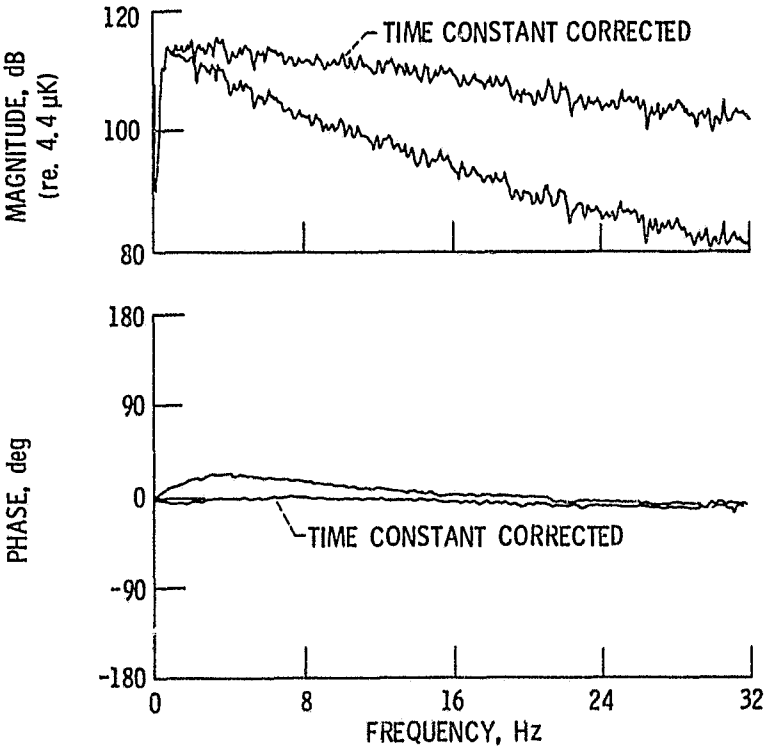

Figure 4. - Two wire chromel alumel thermocouple time constant determination: temperature cross-spectrum between thick and thin thermocouples, G_{12} (station 4, T_{INLET} = 875 K, T_{EXIT} = 990 K, W = 0.5 kg/s, bandwidth = 0.08 Hz).

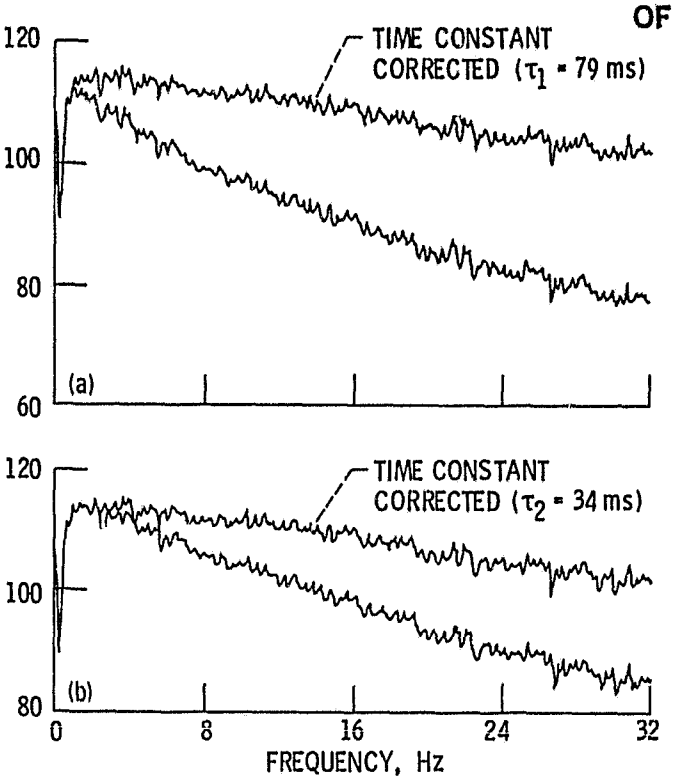

(a) 76.2 μm diameter (G_{11}).

(b) 25.4 μm diameter (G_{22}).

Figure 5. - Two wire chromel alumel thermocouple time constant determination: temperature autospectrum of thick and thin thermocouples (station 4, T_{INLET} = 875 K, T_{EXIT} = 990 K, W = 0.5 kg/s, bandwidth = 0.08 Hz).

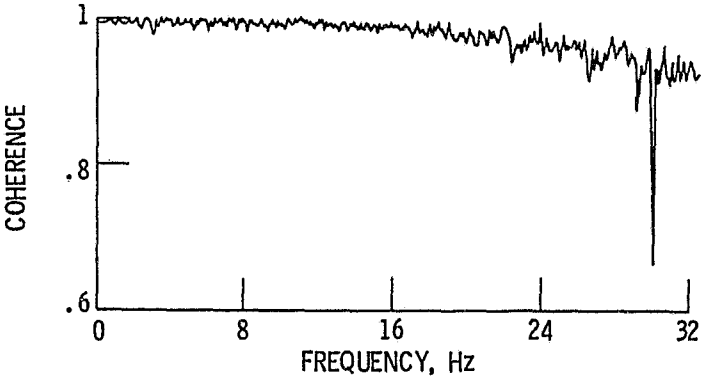

Figure 6. - Two wire chromel alumel thermocouple time constant determination: temperature coherence between thick and thin thermocouples (station 4, T_{INLET} = 875 K, T_{EXIT} = 990 K, W = 0.5 kg/s, bandwidth = 0.08 Hz).

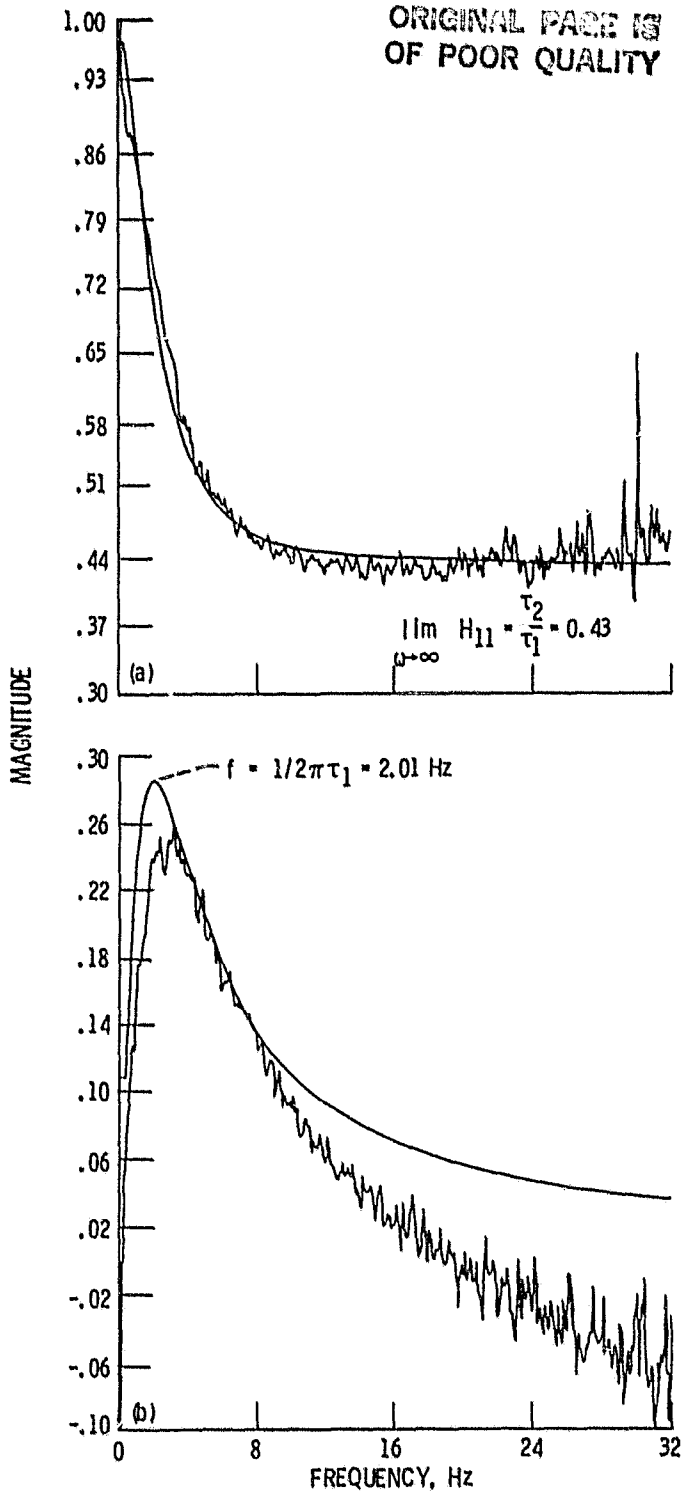

(a) Real part of H_{11}.
(b) Imaginary part of H_{11}.

Figure 7. - Two wire chromel alumel thermocouple time constant determination: thick thermocouple ratio, $H_{11} = G_{11}/G_{12}$ (station 4, T_{INLET} = 875 K, T_{EXIT} = 990 K, W = 0.5 kg/s, bandwidth = 0.08 Hz).

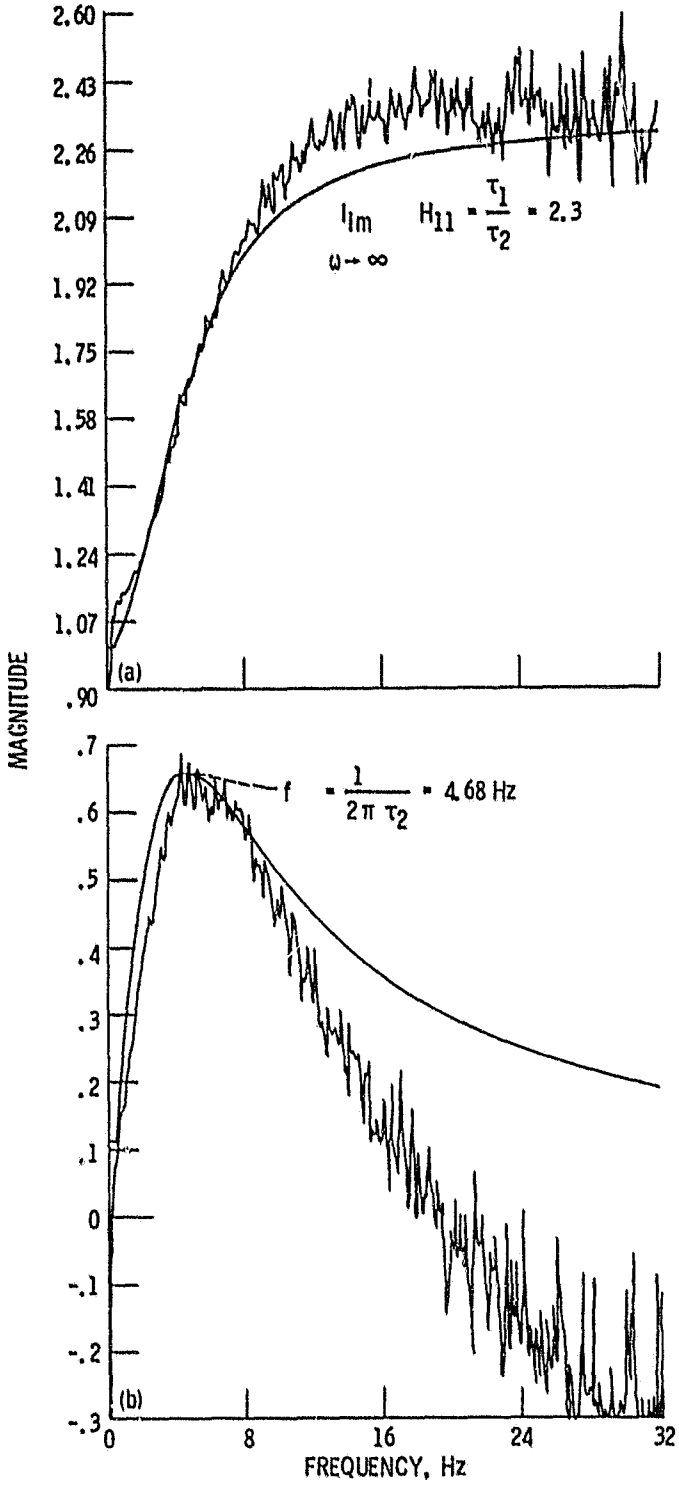

(a) Real part of H_{22}.
(b) Imaginary part of H_{22}.

Figure 8. - Two wire chromel alumel thermocouple time constant determination: thin thermocouple ratio, $H_{22} = G_{11}/G_{12}$ (station 4, T_{INLET} = 875 K, T_{EXIT} 6 990 K, W = 0.5 kg/s, bandwidth = 0.08 Hz).

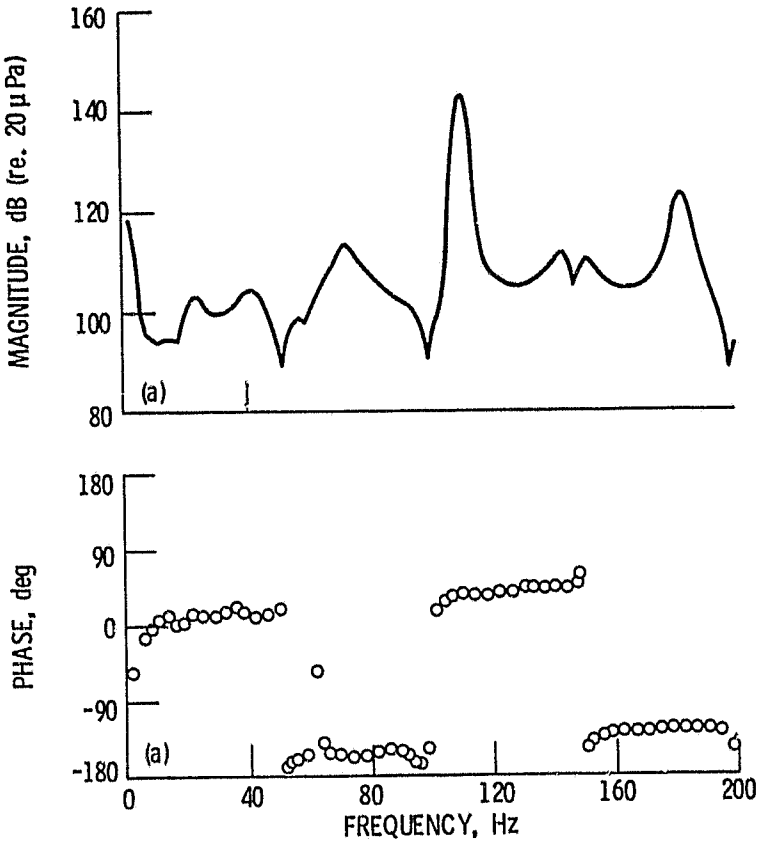

(a) T_{INLET} = 1115 K, T_{EXIT} = 1135 K, W = 0.5 kg/s.

Figure 9. - Pressure cross-spectra between duct inlet (station 3) and duct exit (station 4), $p_4 p_3^*$ (bandwidth = 2 Hz).

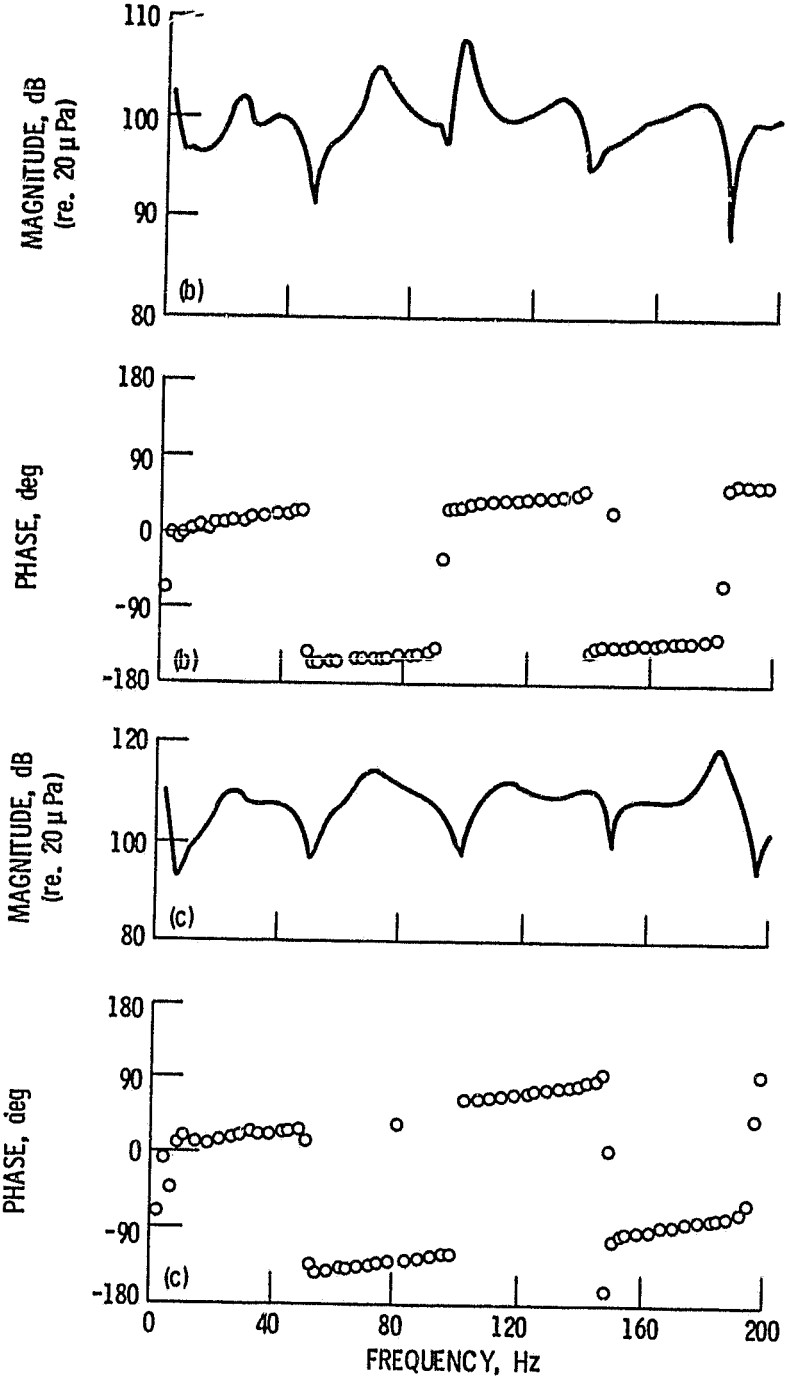

(b) T_{INLET} = 875 K, T_{EXIT} = 990 K, W = 0.5 kg/s.
(c) T_{INLET} = 920 K, T_{EXIT} = 1120 K, W = 1.13 kg/s.

Figure 9. - Concluded.

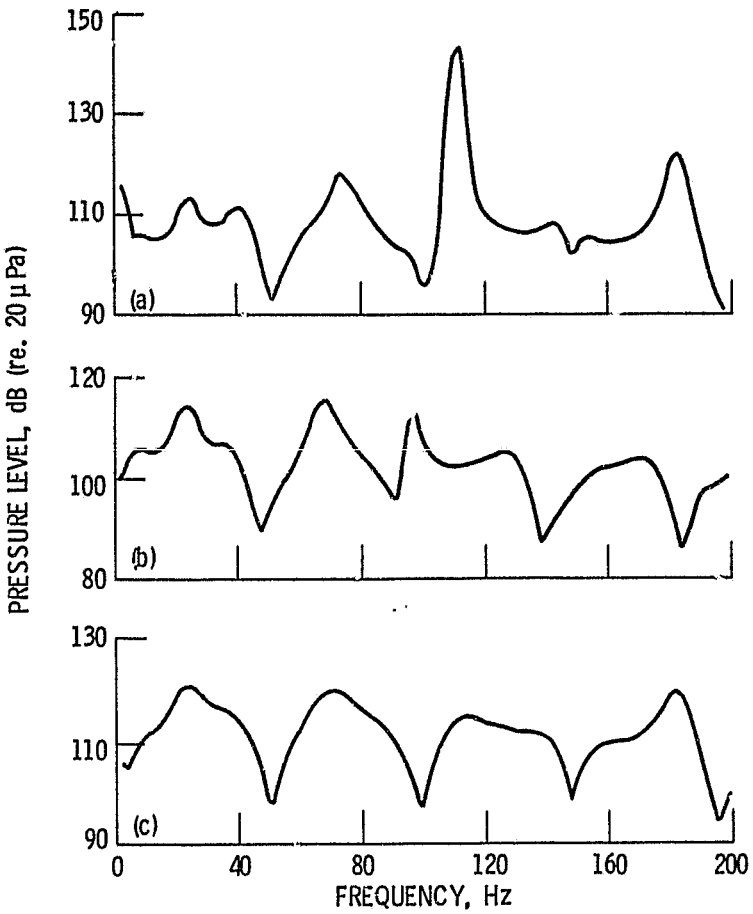

(a) T_{INLET} = 1115 K, T_{EXIT} = 1135 K, W = 0.5 kg/s.
(b) T_{INLET} = 875 K, T_{EXIT} = 990 K, W = 0.5 kg/s.
(c) T_{INLET} = 920 K, T_{EXIT} = 1120 K, W = 1.13 kg/s.

Figure 10. - Pressure auto-spectra near duct inlet (station 3), $p_3\, p_3^*$ (bandwidth = 2 Hz).

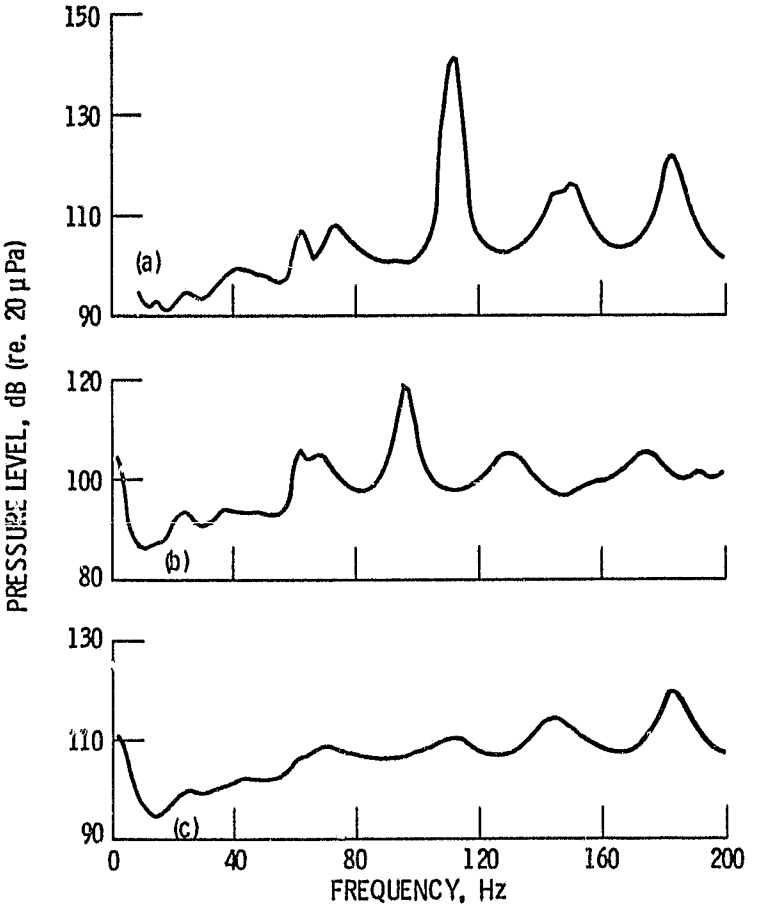

(a) T_{INLET} = 1115 K, T_{EXIT} = 1135 K, W = 0.5 kg/s.
(b) T_{INLET} = 875 K, T_{EXIT} = 990 K, W = 0.5 kg/s.
(c) T_{INLET} = 920 K, T_{EXIT} = 1120 K, W = 1.13 kg/s.

Figure 11. - Pressure auto-spectra near duct exit (station 4), $p_4 p_4^*$ (bandwidth = 2 Hz).

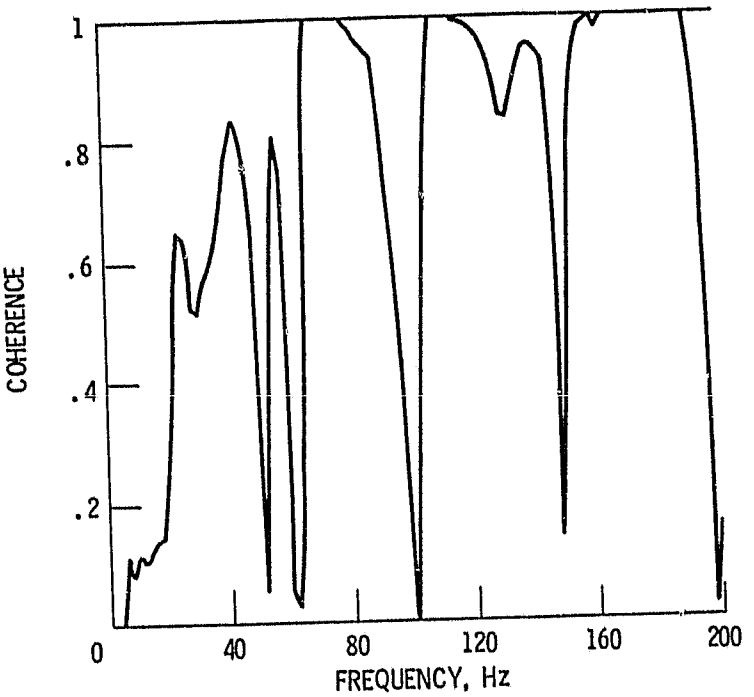

Figure 12. - Pressure coherence between duct inlet (station 3) and duct exit (station 4), $|p_4 p_3^*|^2 / |p_3|^2 |p_3|^2$ (bandwidth = 2 Hz).

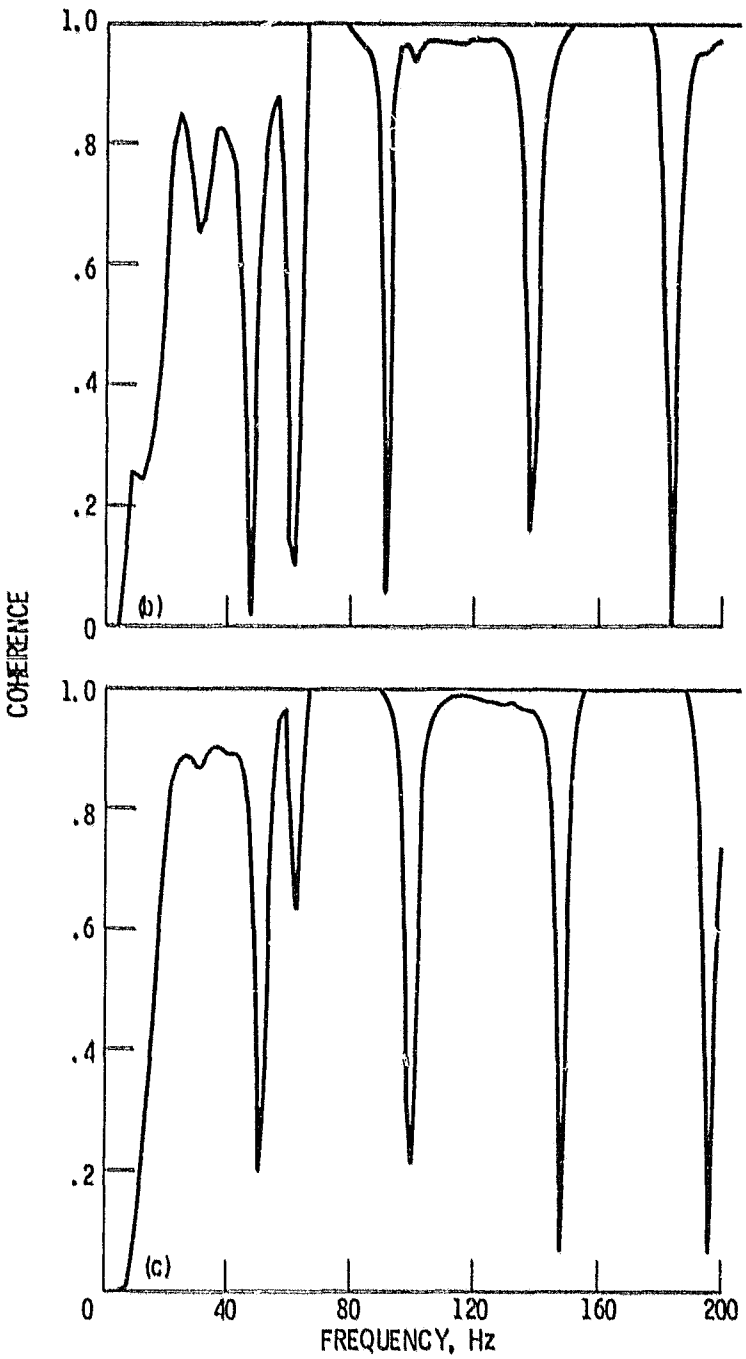

(b) T_{INLET} = 875 K, T_{EXIT} = 990 K, W = 0.5 kg/s.
(c) T_{INLET} = 920 K, T_{EXIT} = 1120 K, W = 1.13 kg/s.

Figure 12. - Concluded.

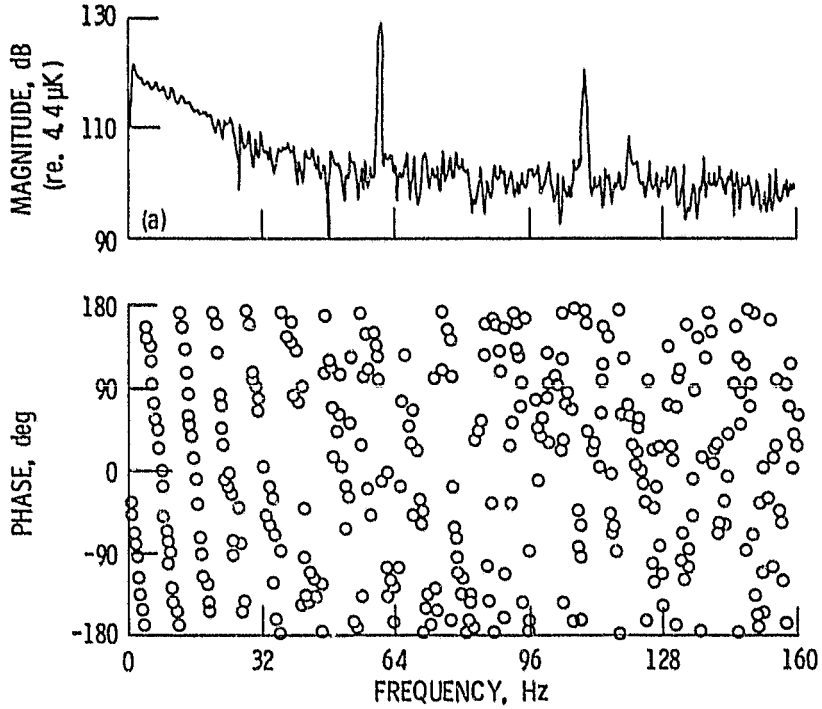

(a) T_{INLET} = 1115 K, T_{EXIT} = 1135 K, W = 0.5 kg/s.

Figure 13. - Temperature cross-spectra between duct inlet (station 3) and duct exit (station 4), $T_4T_3^*$ (bandwidth = 0.4 Hz).

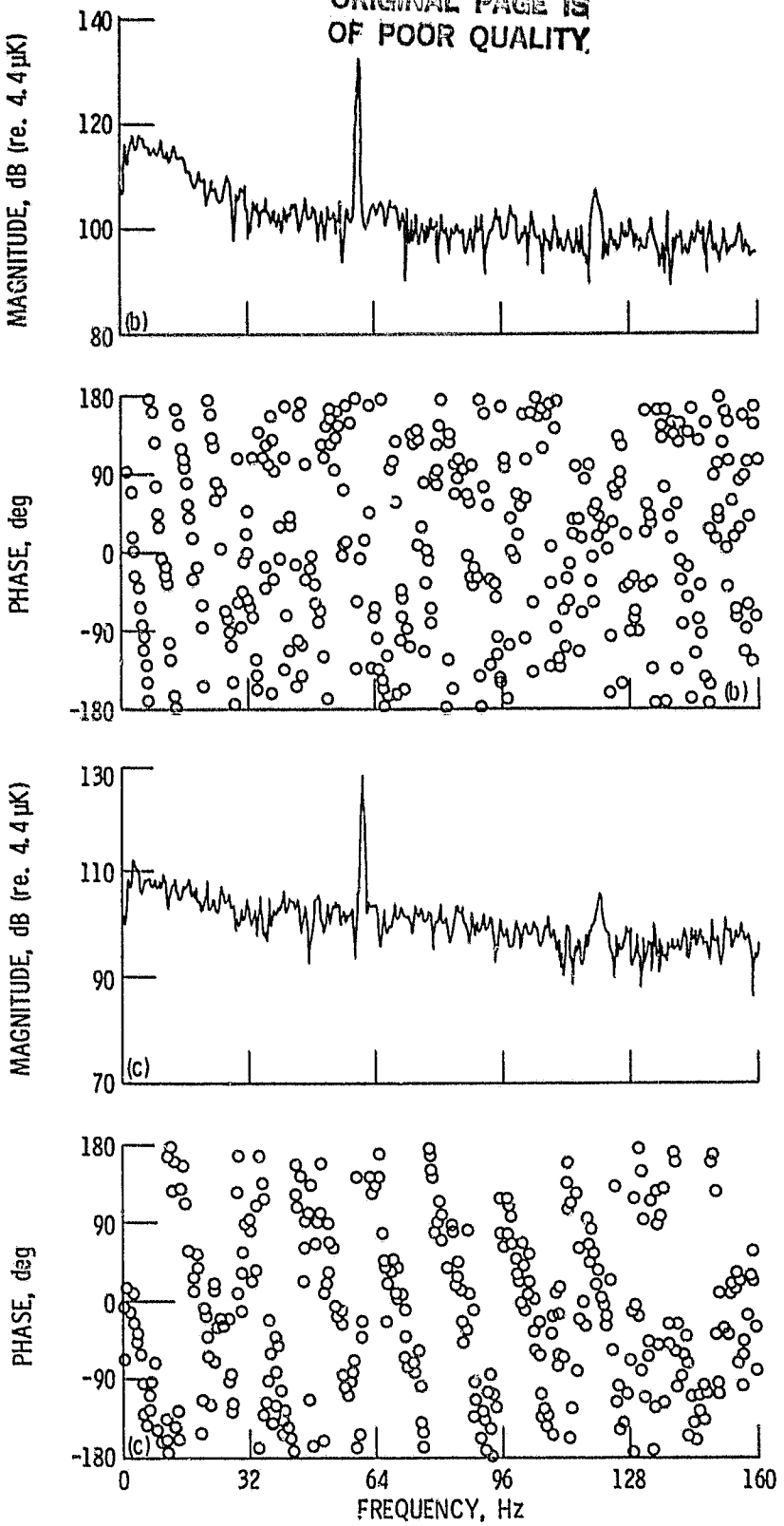

(b) T_{INLET} = 875 K, T_{EXIT} = 990 K, W = 0.5 kg/s.
(c) T_{INLET} = 920 K, T_{EXIT} = 1115 K, W = 1.13 kg/s.

Figure 13. - Concluded.

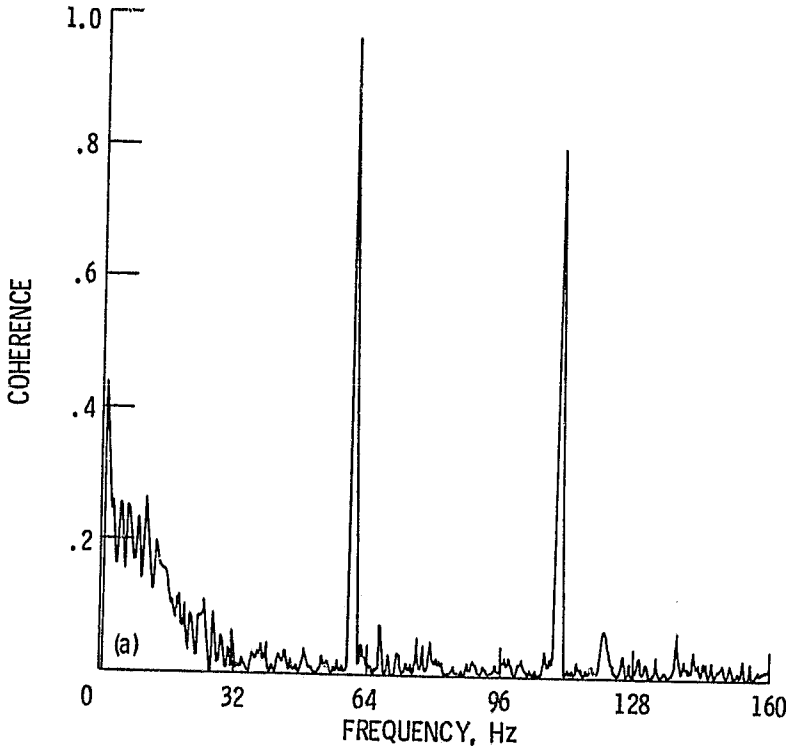

(a) T_{INLET} = 1115 K, T_{EXIT} = 1135 K, W = 0.5 kg/s.

Figure 14. - Temperature coherence between duct inlet (station 3) and duct exit (station 4), $|T_4T_3^*|/|T_y|^2|T_3|^2$ (bandwidth = 0.4 Hz).

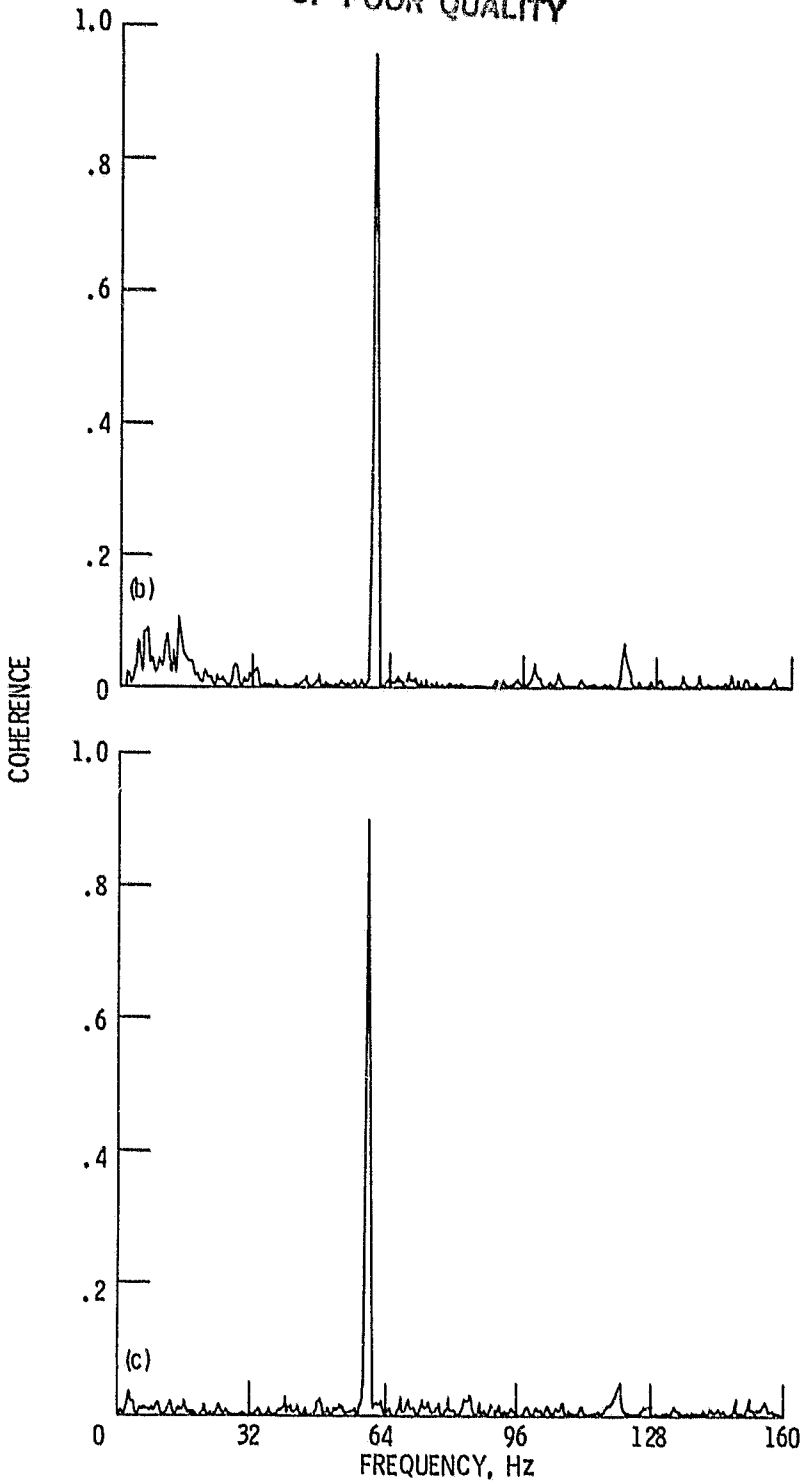

(b) T_{INLET} = 875 K, T_{EXIT} = 990 K, W = 0.5 kg/s.
(c) T_{INLET} = 920 K, T_{EXIT} = 1120 K, W = 1.13 kg/s.

Figure 14. - Concluded.

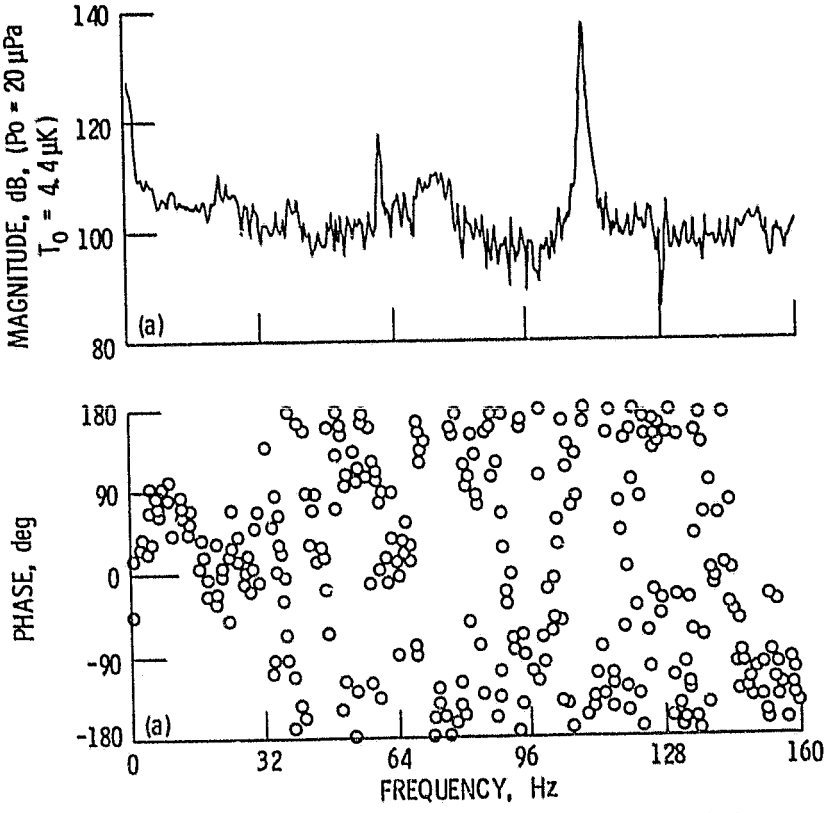

(a) T_{INLET} = 1115 K, T_{EXIT} = 1135 K; W = 0.5 kg/s.

Figure 15. - Cross-spectra between pressure and temperature at duct inlet (station 3), $p_3 T_3^*$ (bandwidth = 0.4 Hz).

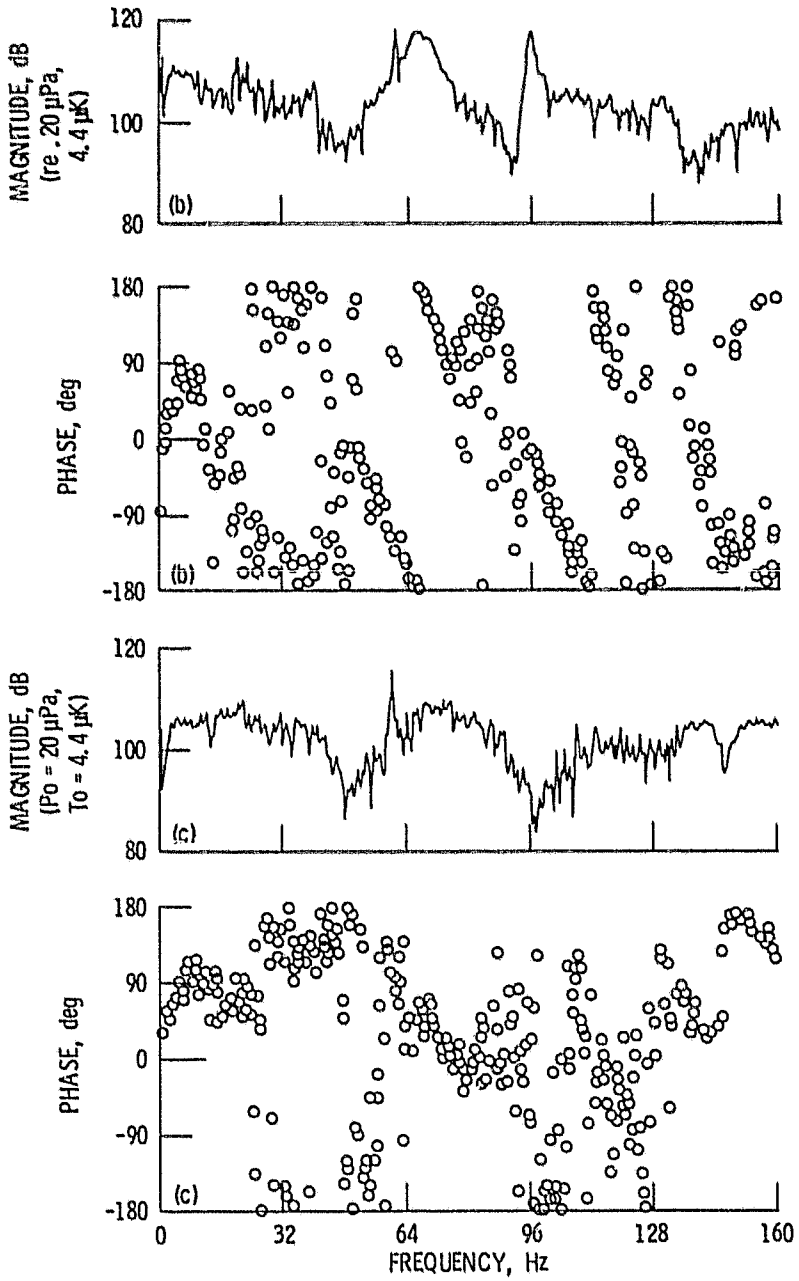

(b) T_{INLET} = 875 K, T_{EXIT} = 990 K, W = 0.5 kg/s.
(c) T_{INLET} = 920 K, T_{EXIT} = 1120 K, W = 1.13 kg/s.

Figure 15. - Concluded.

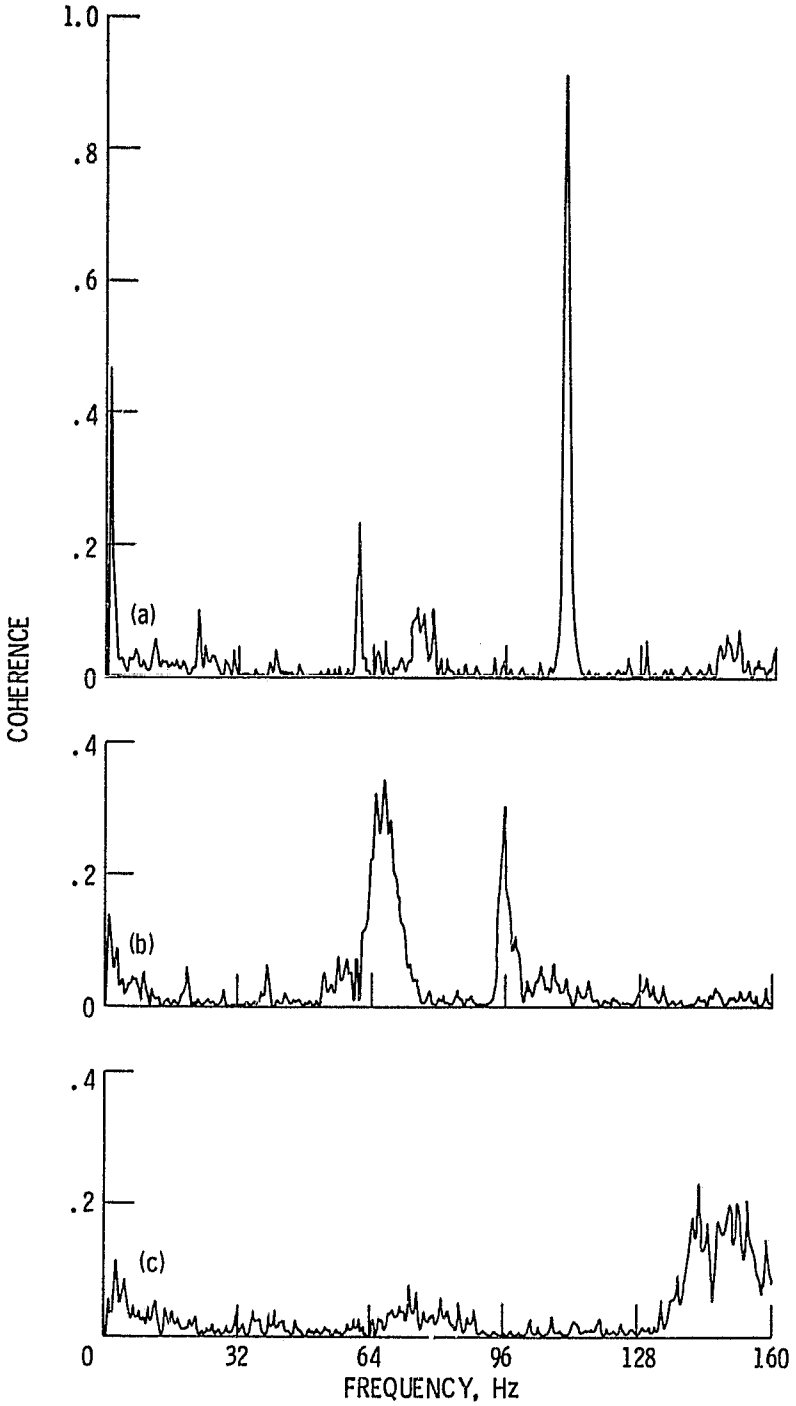

(a) T_{INLET} = 1115 K, T_{EXIT} = 1135 K, W = 0.5 kg/s.
(b) T_{INLET} = 875 K, T_{EXIT} = 990 K, W = 0.5 kg/s.
(c) T_{INLET} = 920 K, T_{EXIT} = 1120 K, W = 1.13 kg/s.

Figure 16. - Coherence between pressure and temperature at duct inlet (station 3), $|p_3 T_3^*|^2 / |T_3|^2 |p_3|^2$ (bandwidth = 0.4 Hz).

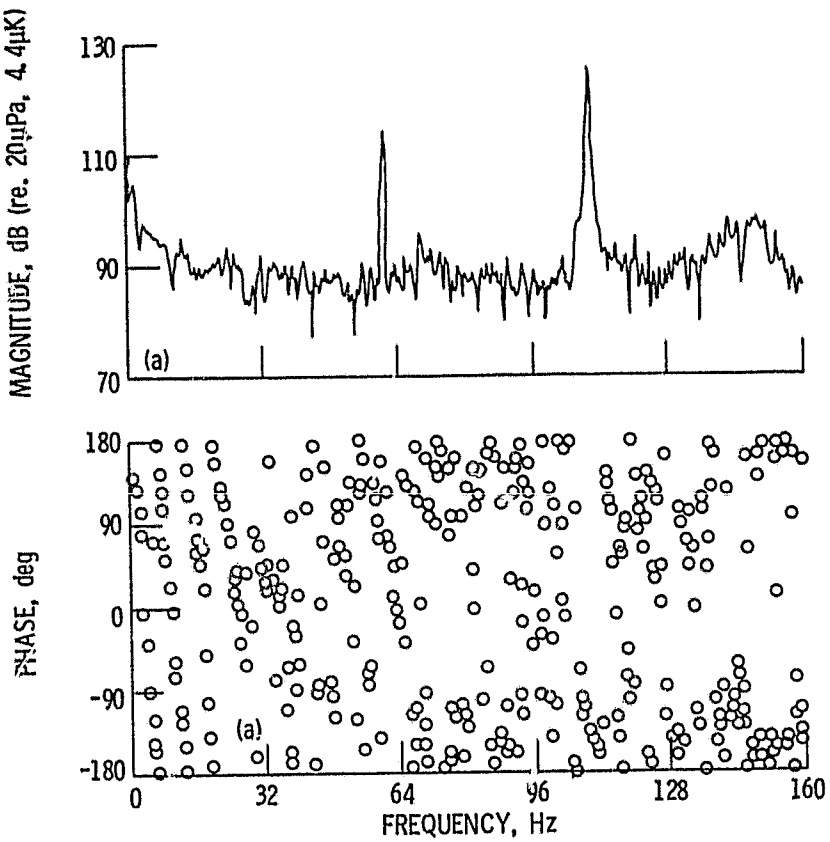

(a) T_{INLET} = 1115 K, T_{EXIT} = 1135 K, W = 0.5 kg/s.

Figure 17. - Cross-spectra between pressure and temperature at duct exit (station 4), $p_4 T_4^*$ (bandwidth = 0.4 Hz).

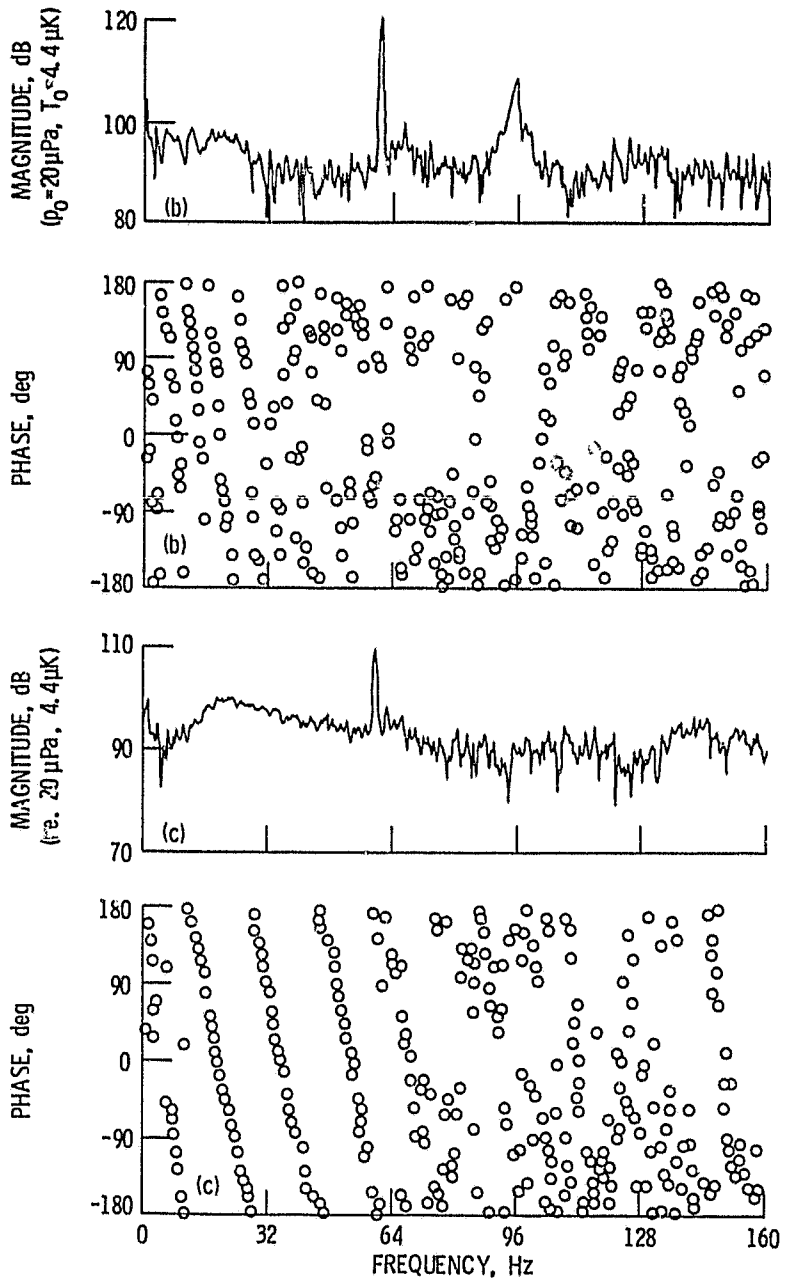

(b) T_{INLET} = 875 K, T_{EXIT} = 990 K, W = 0.5 kg/s.
(c) T_{INLET} = 920 K, T_{EXIT} = 1120 K, W = 1.13 kg/s.

Figure 17. - Concluded.

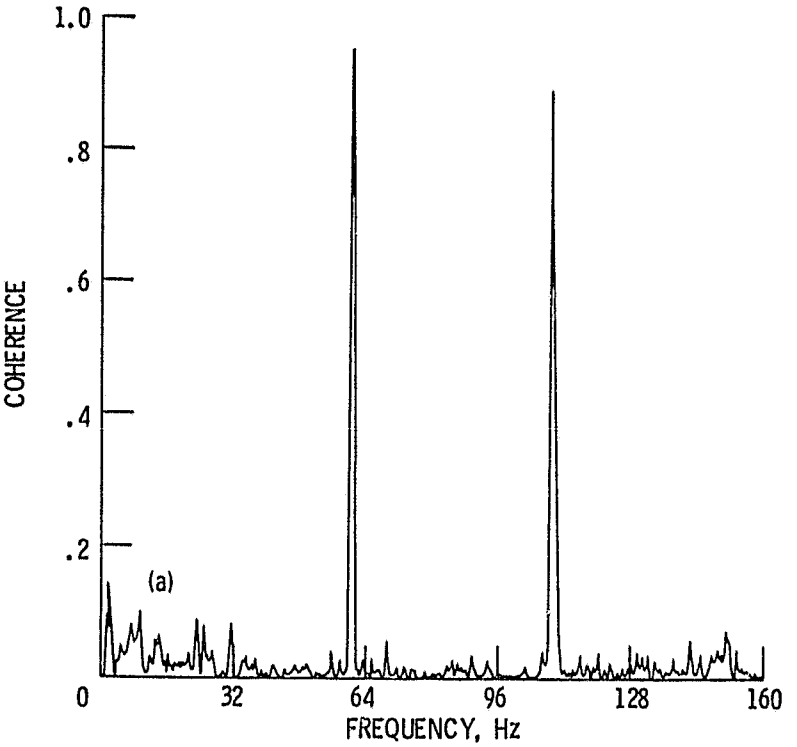

(a) T_{INLET} = 1115 K, T_{EXIT} = 1135 K, W = 0.5 kg/s.

Figure 18. - Coherence between pressure and temperature at duct exit (station 4), $|p_4 T_4^*|^2 / |T_4|^2 |p_4|^2$ (bandwidth = 0.4 Hz).

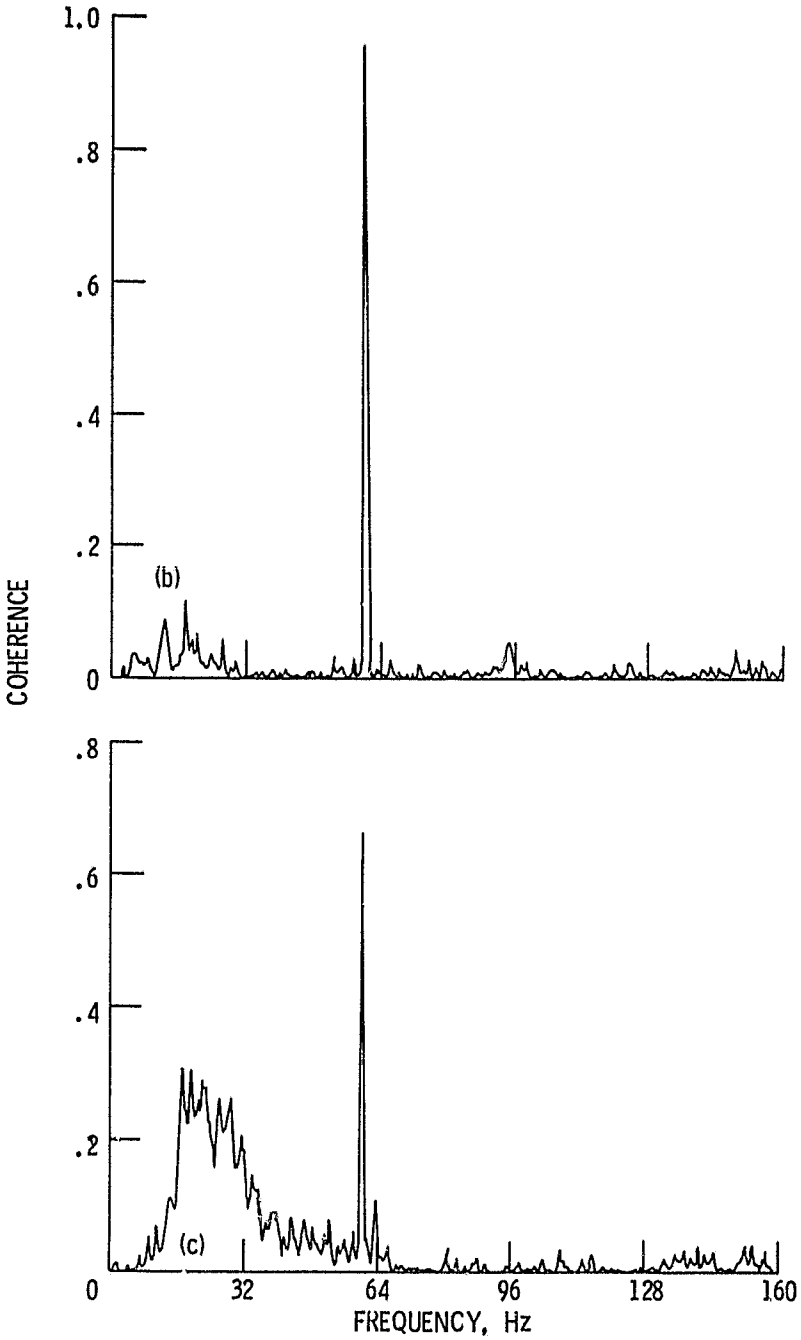

(b) T_{INLET} = 875 K, T_{EXIT} = 990 K, W = 0.5 kg/s.
(c) T_{INLET} = 920 K, T_{EXIT} = 1120 K, W = 1.13 kg/s.

Figure 18. - Concluded.